

Intracellular Kinetics of a Growing Virus: A Genetically Structured Simulation for Bacteriophage T7

Drew Endy, Deyu Kong, John Yin

Thayer School of Engineering, Dartmouth College, Hanover, New Hampshire 03755-8000; telephone: (603) 646-3193; fax: (603) 646-3856; e-mail: jyin@dartmouth.edu

Received 13 September 1996; accepted 20 December 1996

Abstract: Viruses have evolved to efficiently direct the resources of their hosts toward their own reproduction. A quantitative understanding of viral growth will help researchers develop antiviral strategies, design metabolic pathways, construct vectors for gene therapy, and engineer molecular systems that self-assemble. As a model system we examine here the growth of bacteriophage T7 in *Escherichia coli* using a chemical-kinetic framework. Data published over the last three decades on the genetics, physiology, and biophysics of phage T7 are incorporated into a genetically structured simulation that accounts for entry of the T7 genome into its host, expression of T7 genes, replication of T7 DNA, assembly of T7 procapsids, and packaging of T7 DNA to finally produce intact T7 progeny. Good agreement is found between the simulated behavior and experimental observations for the shift in transcription capacity from the host to the phage, the initiation times of phage protein synthesis, and the intracellular assembly of both wild-type phage and a fast-growing deletion mutant. The simulation is utilized to predict the effect of antisense molecules targeted to different T7 mRNA. Further, a postulated mechanism for the down regulation of T7 transcription in vivo is quantitatively examined and shown to agree with available data. The simulation is found to be a useful tool for exploring and understanding the dynamics of virus growth at the molecular level. © 1997 John Wiley & Sons, Inc. *Biotechnol Bioeng* 55: 375–389, 1997.

Keywords: bacteriophage T7; kinetic simulation; intracellular growth; gene expression; antiviral strategies

INTRODUCTION

The growth of a virus in its host cell is a complex and highly orchestrated multimolecular process. In seeking to understand this process, the disciplines of biochemistry, molecular biology, and biophysics have illuminated structures and functions for the essential genetic and protein components of numerous viruses. Yet, it remains a challenge to quantify how these components influence the overall dynamics of viral growth. For example, if a virus is modified to express an RNA polymerase that transcribes half as fast as the wild-type enzyme, how much slower will it grow? How would

this change affect the expression of a recombinant gene carried by the virus? From a biomedical perspective, which will more effectively inhibit a retrovirus, a ribozyme that targets the mRNA of the viral reverse transcriptase or one that targets the integrase mRNA? These are difficult questions to address because they attempt to intuit how a change in any component of a complex system would influence the overall system behavior.

A kinetic simulation can provide a starting point toward understanding the system dynamics of viral growth. By consolidating and organizing the available information for the synthesis and assembly of a virus in a kinetic framework, at least three benefits should emerge. First, if a simulation is based on published mechanisms and data, it can examine the consistency of these data and reveal when new findings challenge the existing literature. Mismatches between experimentally measured and simulated results then provide the investigator with an opportunity to revise his or her understanding of the process. Second, the simulation can predict the in vivo effects of selected antiviral strategies on overall growth dynamics. Since a simulation is readily modified, many potential strategies can be explored before one sets foot in the laboratory or clinic. Finally, a kinetic simulation of viral growth may benefit engineers who seek to gain insights from nature for the design of nanoscale processes capable of molecular recognition, catalysis, and self-assembly.

Previous simulations have examined aspects of viral growth from a variety of perspectives. These include the effect of receptor blocking and binding site inactivation on human rhinovirus (HRV) and human immunodeficiency virus (HIV-1) binding to cell surfaces (Wickham et al., 1995); the binding, entry, uncoating, and total RNA synthesis for a Semliki Forest virus infection (Dee et al., 1995); the dynamic feedback mechanisms and the virus–cell interaction of HIV-1 (Hammond, 1993; Palsson et al., 1990; Ruggiero et al., 1994); the phases of phage Q β replication (Eigen et al., 1991); the system connectivity and feedback control in phage lambda (McAdams and Shapiro, 1995); the assembly of icosahedral virus capsids (Zlotnick, 1994); and the lag time effect of DNA insertion in phage T3 and T7 (Buchholtz and Schneider, 1987). The T3/T7 model of Buchholtz

Correspondence to: J. Yin

Contract grant sponsor: National Science Foundation

and Schneider utilized a minimal transcription and translation system to examine the effect of DNA entry rate on phage gene expression, while adjusting parameters to fit the observed expression of three T7 proteins and DNA replication.

Here, we have assembled and incorporated mechanistic and kinetic data from the literature to simulate the T7 infection cycle, from T7 DNA insertion to progeny formation. By employing experimentally determined, rather than fitted, parameters wherever possible, the simulation will provide a stronger foundation for exploring T7 growth. As shown in Figure 1, our simulation takes as input the mechanisms and rates for DNA entry, mRNA synthesis, protein (gene product, gp) synthesis, DNA replication, and phage assembly. As output the simulation predicts in vivo concentrations for each component of the phage during its growth cycle, including the formation of phage progeny. The approach may be extended to explore potential antiviral strategies by defining additional reactions representing specific antiviral agents.

We focus on bacteriophage T7 as our model system because its study over the last half century (Demerec and Fano, 1944) provides an extensive data base from which to develop the simulation. In addition, phage T7 has served in

recent years as a model system for viral evolution (Hillis et al. 1992; Lee & Yin, 1996; Yin, 1993). T7 is a lytic phage that infects *Escherichia coli*, producing approximately 100 progeny per infected cell within 40 min at 30°C. Detailed descriptions of the T7 genome and growth cycle (Dunn and Studier, 1983; Studier and Dunn, 1983) provide the biological foundation for our simulation. The sequenced T7 genome of 39,937 bp codes for 56 genes which produce 52 known proteins. The genes are grouped into three classes based on function and position. The class I genes moderate the transition in metabolism from host to phage. Class II genes are responsible for T7 DNA replication, and class III genes code for particle, maturation, and packaging proteins. The growth cycle is initiated when the phage binds to the host, which is followed by translocation of the linear double-stranded T7 DNA molecule into the cell. Although other phages such as lambda inject their DNA within 1 min, the entry of T7 DNA takes about 10 min (Garcia and Molineux, 1995; Zavriev and Shemyakin, 1982) and thereby influences the sequential expression of T7 genes. Transcription of class I genes (Fig. 2A) is catalyzed by *E. coli* RNA polymerase (EcRNAP), which recognizes three promoters positioned near the entering end of the T7 DNA. Once the T7-specific RNA polymerase (gp1) is expressed, it transcribes the class II (Fig. 2B) and class III (Fig. 2C) genes. In vitro data suggest transcription of later genes is influenced by an increase in gp1 promoter strengths from the class II to class III DNA (Ikeda, 1992). Further, the T7 lysozyme (gp3.5) binds gp1, causing a reduction in transcription at about the time T7 DNA replication begins (Zhang and Studier, 1995). Replicated DNA is packaged into procapsids and supplemented with several other phage particle proteins to form progeny, which are then released into the environment by abrupt lysis of the host (Hausmann, 1988; Young, 1992).

MATERIALS AND METHODS

Phage and Bacteria Cultures

Escherichia coli BL21 and BL21(DE2) (described in Studier and Moffatt, 1986) as well as wild-type bacteriophage T7 (T7-WT) were generously provided by F. W. Studier (Brookhaven National Laboratory, NY). BL21(DE2) constitutively expresses T7 gene *l*. Bacteriophage T7 $\Delta 0.7-1$ (T7-26) was obtained from earlier work (Kong and Yin, 1995). Established methods were used in the preparation, preservation, and assay of the phage and bacteria (Adams, 1959; Miller, 1972; Studier, 1969). All growth media, buffers and agars were prepared using distilled water. T-broth containing 10 g/L Bacto-tryptone (Difco, Detroit, MI) and 5 g/L NaCl was used as growth medium for overnight and shaker cultures. Bottom agar for plates and soft agar for overlays were T-broth containing 1.0% and 0.7% Bacto-agar (Difco), respectively. Phage dilutions were performed in buffer containing 10 mM Tris-HCl (pH 7.5), 1 mM MgCl₂, 0.1 M NaCl, 10 mg/L gelatin, and 10 mM CaCl₂.

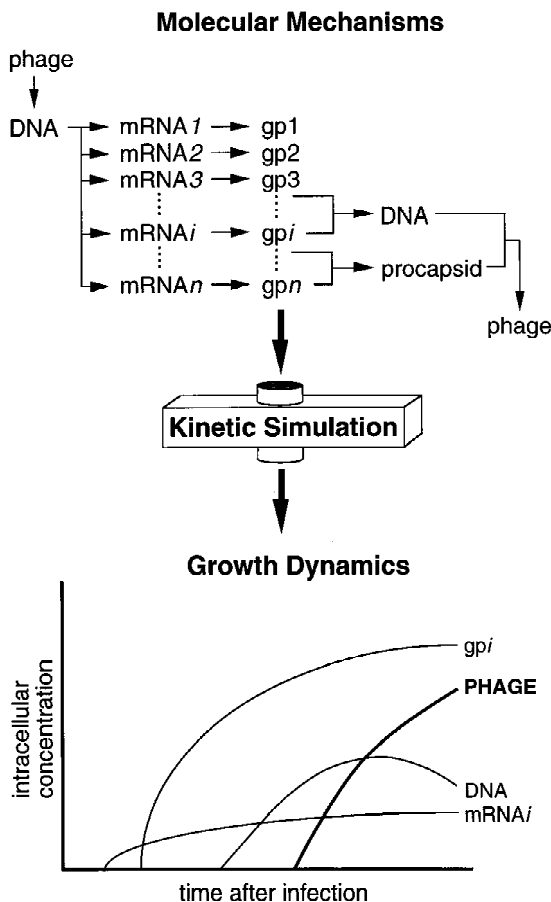


Figure 1. Kinetic simulation utilizes mechanisms and rate data from single reactions to create a coupled system of equations capable of predicting the overall intracellular dynamics of the phage infection.

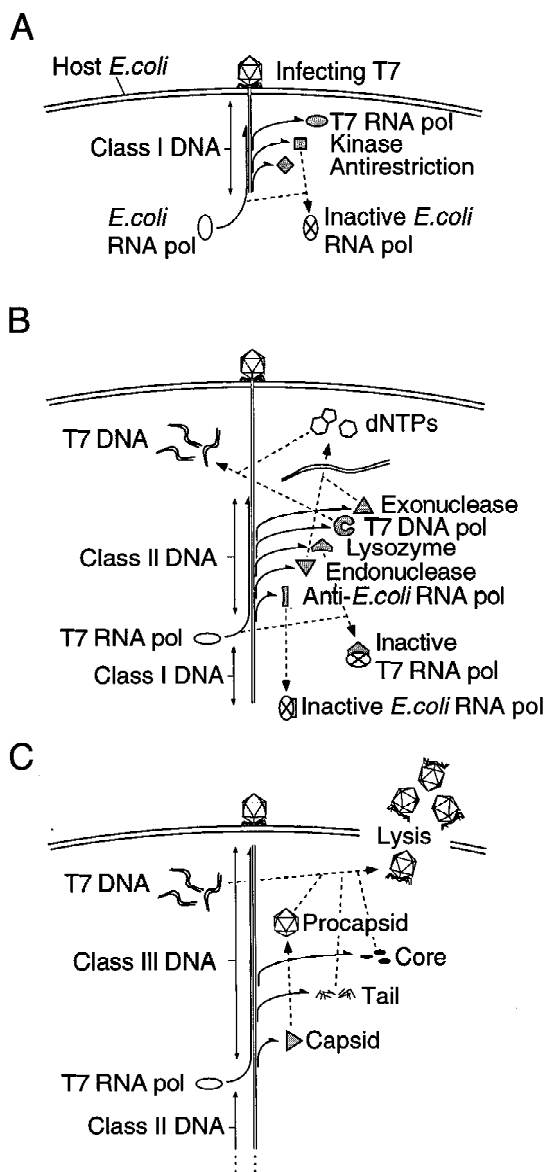


Figure 2. Growth cycle of phage T7. The solid lines with half arrows indicate transcription and translation, the dashed lines denote reaction, and the solid lines with full arrows mark the three classes of T7 DNA. (A) Class I DNA expression, infection initiation. (B) Class II DNA expression, phage DNA replication machinery. (C) Class III DNA expression, phage particle and packaging proteins.

Wild-type bacteriophage stock was prepared as follows: 200 μL of an BL21 overnight culture grown in T-broth was added to 25 mL of fresh T-broth and incubated at 37°C on a shaker table at 150 rpm. After 6 h, phage were added at a multiplicity of infection of 10^{-3} . Upon lysis, the solution was brought up to 1 M NaCl and allowed to remain at room temperature for 1 h. The culture was filtered with sterile 0.2- μm UNIFLO® filters (Schleicher & Schuell, Keene, NH) to remove cell debris and stored at 4°C until use.

One-Step Growth

Two hundred microliters of an BL21 overnight culture grown in T-broth was added to 25 mL of fresh T-broth and

incubated at 30°C on a shaker table at 150 rpm. After 6 h (*E. coli* growth rate of approximately 1 doubling per hour, data not shown) phage were added at a multiplicity of infection of 10^{-2} . Five minutes after inoculation with phage, 200 μL of the shaker culture was transferred into 20 mL of fresh T-broth to minimize further binding of phage to bacteria. Subsequent samples taken during the growth cycle were diluted (10–20-fold) into phage buffer saturated with chloroform (International Biotechnologies, New Haven, CT) to liberate intracellular phage. After 30 s samples were further diluted (10–20-fold) and stored in phage buffer at 1°C. At the end of the growth cycle, samples were diluted as required and plated out on BL21. Plaque titers were determined by counting after 4–6 h of incubation at 37°C.

Numerical Simulation

The system of ordinary differential equations was solved using a fourth-order Runge–Kutta algorithm (Burden and Faires, 1993). Computation time for the T7-WT growth cycle (0.1-s time-step) was approximately 20 s using a 180-MHz SGI R5000 with a floating-point coprocessor. The simulation was coded in FORTRAN.

SIMULATION

The intracellular T7 growth cycle is simulated with a system of coupled ordinary differential equations that is solved numerically. The kinetic rates and binding constants used in the simulation are summarized in Table I. The rates for amino acid chain elongation and procapsid assembly have been converted to 30°C assuming a rate doubling for a 10°C increase. The simulation begins with entry of the infecting T7 DNA into the host and continues through phage particle assembly. Lysis of the host cell is not included in the simulation.

Translocation of T7 DNA from Infecting Particle to Host

Entry of T7 DNA into the host cell occurs in several distinct stages (Garcia and Molineux, 1995; Moffatt and Studier, 1988; Zavriev and Shemyakin, 1982). The first stage involves the ejection of approximately 1000 bp from the infecting particle. This section of T7 DNA contains three EcRNAP promoters: A1, A2, and A3. As these promoters are recognized by EcRNAP, transcription of the class I genes begins and the T7 DNA is pulled into the cell by the elongating EcRNAP. Once gene 1 is expressed and the resulting gp1 recognizes the first class II gp1 promoter, ϕI_{1A} , translocation occurs at the faster gp1 elongation rate until the entire T7 genome enters the host. Translocation is simulated by starting with an ejection rate of 5 bps (base pairs per second) until A1 enters the host. Then, EcRNAP-mediated translocation occurs at 40 bps until ϕI_{1A} enters

Table I. Simulation parameters.

Parameter	Value	Reference
Kinetic		
Infecting DNA insertion	5,40, and 200 bps ^a	Garcia and Molineux, 1995; Zavriev and Shemyakin, 1982
Transcription, <i>E. coli</i> RNA polymerase	$k_{ph} = 40$ nucleotides/s/RNAP	Bremer and Yuan, 1968; Rose et al., 1970
Transcription, T7 RNA polymerase	$k_{pT7} = 200\text{--}300^b$ (as above)	Garcia and Molineux, 1995; Zavriev and Shemyakin, 1982
T7 mRNA decay	$k_{dm} = 0/\text{sec}$	Summers, 1970
Translation	$k_R = 14$ AA/sec/ribosome ^c	Dalbaw and Young, 1975
Protein decay	$k_{dgp} = 2.8 \times 10^{-5}/\text{s}^d$	Lee and Bailey, 1984
<i>E. coli</i> DNA degradation	32,357 nucleotides/s ^d	Berlyn et al., 1996; Sadowski and Kerr, 1970
T7 DNA replication	$k_{pD} = 370$ bps/polymerase	Rabkin and Richardson, 1990
DNA packaging	$k_{pk} = 0.702/\text{min}$	Son et al., 1993
Procapsid assembly	$k_{as} = 4.6 \times 10^{-16}/(\text{number}/\text{cell})^{3.78}/\text{min}^{e,d}$	Prevelige et al., 1993
Binding		
<i>E. coli</i> RNA polymerase and gp2	$K_{eq1} = 5.0 \times 10^7/M^d$	Hesselbach and Nakada, 1977a
<i>E. coli</i> RNA polymerase and gp0.7	$K_{eq2} = 5.5 \times 10^6/M^e$	Hesselbach and Nakada, 1977b
T7 RNA polymerase and gp3.5	$K_{eq3} = 1.5 \times 10^7/M^d$	Ikeda and Bailey, 1992
Other		
T7 promoter strengths	Table II	Ikeda, 1992
T ϕ terminator efficiency	$\eta_{T\phi} = 0.66$	Macdonald et al., 1993
Total <i>E. coli</i> RNA polymerase	1800 molecules/cell	Bremer and Yuan, 1968
RNA polymerase spacing requirement	$S_p = 233/\mu^2 + 73$ bp	Dennis and Bremer, 1973, 1974
Ribosomal spacing requirement	$S_r = 82.5/\mu + 145$ nucleotides	Dennis and Bremer, 1973, 1974
K_m for DNA elongation	$K_m = 8668$ nucleotides/cell	Donlin and Johnson, 1994
Nucleation level, procapsid assembly	$C_N = 3036$ molecules/cell ^d	Prevelige et al., 1993
T7 particle protein stoichiometry	See Nomenclature	Steven and Trus, 1986
<i>E. coli</i> volume	$8 \times 10^{-16}\text{L}$	Donachie & Robinson, 1987

^abps = base pairs per second.

^b200 bps used.

^cRate is corrected to 30°C.

^dDerived from published data.

^eFit to published data.

and the translocation rate increases to 200 bps. We assume that both EcRNAP and gp1 are able to immediately recognize their respective promoters and effect translocation. Using these mechanisms, the length of inserted T7 DNA is calculated at each point in time until the entire genome enters the cell.

Transcription of T7 DNA

The simulation accounts for the synthesis of complete transcripts from gene i once the entire coding region for gene i has entered the host. The values of i , which are not necessarily integer, range from 0.3 to 19.5 as previously defined (Studier and Dunn, 1983). Although T7 transcripts are polycistronic, the simulation accounts for each gene's mRNA concentration individually because we assume the synthesis rate for each protein has a first-order dependence on its total mRNA concentration. The basic form of the rate equation follows those developed previously for gene expression in *E. coli* (Lee and Bailey, 1984; Shuler et al., 1979). Because of the fast rate for polymerase binding and initiation (Maslak et al., 1993) relative to transit time on the DNA, T7 transcription is simulated by assuming mRNA elongation is the rate-limiting step.

Transcription of the class I genes initiates from the three EcRNAP promoters A1, A2, and A3. Since these promoters

are upstream of the first T7 gene, which codes for an anti-restriction protein (gp0.3), we assume variations in the strengths of these promoters do not lead to variations in the transcription rates among the class I genes. In addition, transcript initiation from the weaker EcRNAP promoters, B and C, is assumed to be insignificant during the T7-WT infection (Dunn and Studier, 1975) and is not included in the simulation. With these assumptions, the rate equation for each class I mRNA depends on its rate of synthesis and decay as follows:

$$\frac{d(\text{mRNA}_i)}{dt} = \left[\frac{(k_{ph})(P_h)}{L_H(t)} \right] - (k_{dm})(\text{mRNA}_i) \quad \text{for } i = 0.3, \dots, 1.3 \quad (1)$$

where mRNA_i is the concentration of gene i mRNA, k_{ph} and P_h are the transcription rate and concentration of EcRNAP, respectively, $L_H(t)$ is the average transcript length produced by EcRNAP, and k_{dm} is the T7 mRNA decay rate. Since the T7 mRNA is stable over the course of the growth cycle (Summers, 1970), k_{dm} is set at zero. The EcRNAP elongation rate is assumed to be constant over the entire length of class I DNA. Here, P_h is calculated by dividing the length of inserted class I DNA by the intermolecular spacing requirement for the polymerase, S_p , and multiplying by the percent fraction of active EcRNAP. The term S_p depends on the *E. coli* growth rate and represents the minimum distance be-

tween two elongating EcrNAP's (Dennis and Bremner, 1973, 1974). The length $L_H(t)$ averages the transcript lengths from each inserted class I promoter assuming equal strengths for A1, A2, and A3:

$$L_H(t) = \sum_{j=1}^{n_H(t)} \left((X(t) - A_j) \frac{1}{n_H(t)} \right) \quad (2)$$

where $X(t)$ is the total length of inserted T7 DNA at time t , $n_H(t)$ is the number of inserted EcrNAP promoters at time t , and A_j is the location of promoter j . The term $X(t) - A_j$ increases until the early terminator, TE, enters the cell, after which time it remains fixed at $TE - A_j$. Figure 3 provides a schematic for this term and the switch from $X(t)$ to TE. Although a small percentage of elongating EcrNAP reads through TE (Studier, 1972), we assume such read-through will not significantly modify the expression levels of the T7 genes and have not included it in the simulation.

For transcription of class II and class III genes, which is carried out by gp1, we account for different gp1 promoter strengths by including an additional term, S_p , representing the combined strength of the gene i 's upstream promoters:

$$S_i = \sum_{j=1}^{n_i} S_{\theta j} / \sum_{j=1}^{n_p(t)} S_{\theta j} \quad \text{for } i = 1.4, \dots, 19.5 \quad (4)$$

$$\frac{d(\text{mRNA}_i)}{dt} = (S_i) \left[\frac{(k_{PT7})(P_{T7})}{L_p(t)} \right] - (k_{dm})(\text{mRNA}_i) \quad \text{for } i = 1.4, \dots, 19.5 \quad (3)$$

where k_{PT7} and P_{T7} are the transcription rate and active concentration of gp1, respectively, and $L_p(t)$ is the weighted transcript length produced by gp1. Note that P_{T7} is initially zero but increases as gene I is expressed during the phage growth cycle. The bracketed component of the first term is the total rate of mRNA synthesis by gp1, in units of T7 mRNA molecules per second per infected cell. This is the same for all class II and class III genes at any time t . Multiplication of this term by each gene's transcription strength, S_p , allocates the transcription resources across the class II and class III DNA. Here, S_i is found by dividing the combined strength of gene i 's upstream promoters by the total strength of all available gp1 promoters:

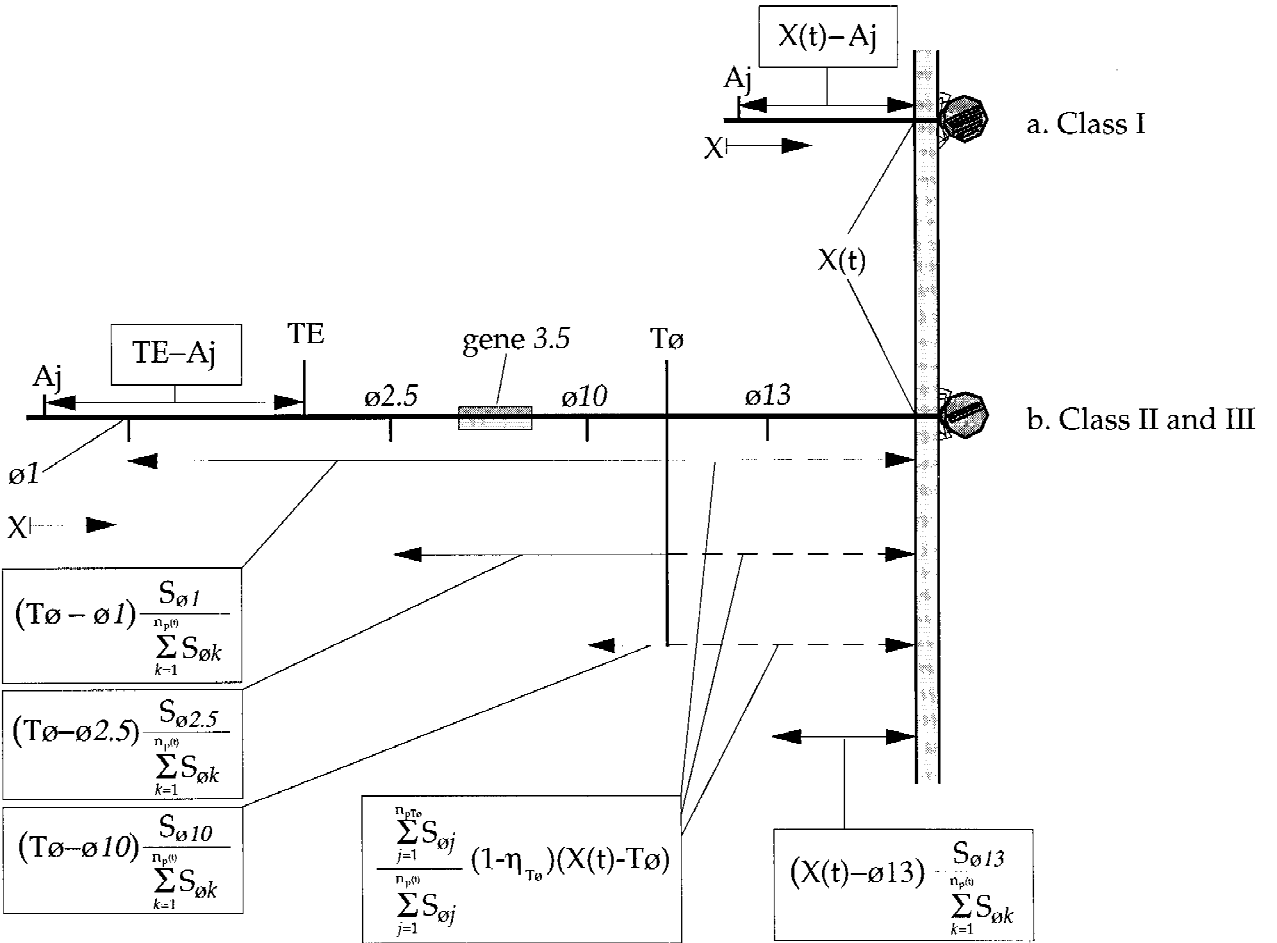


Figure 3. Quantifying the weighted lengths of expressed T7 DNA needed to simulate the allocation of transcription resources. T7 DNA is pictured near (a) the beginning and (b) the end of insertion. For clarity, only four gp1 promoters are shown. Lines bounded by two arrows give the physical basis for the indicated terms from Equations (2) and (5). The dashed lines represent gp1 read-through at T_0 .

where $S_{\phi j}$ is the calculated strength of promoter j , n_i is the number of gp1 promoters upstream of gene i , and $n_p(t)$ is the total number of inserted gp1 promoters at time t . For example, using the simplified T7 genome depicted in Figure 3(b), gene 3.5 has n_i equal to 2 and $n_p(t)$ equal to 4. The values of $S_{\phi j}$ used in the simulation are calculated by multiplying the relative strength of each promoter by its transcript initiation efficiency (Table II).

At any point in time, the weighted transcript length produced by gp1, $L_p(t)$, is calculated by accounting for both the strength of each promoter and the length of the transcript originating from it:

$$L_p(t) = \sum_{j=1}^{n_p(t)} \left((X(t) - \phi j) \frac{S_{\phi j}}{\sum_{k=1}^{n_p(t)} S_{\phi k}} \right) + \frac{\sum_{j=1}^{n_{pT\phi}} S_{\phi j}}{\sum_{j=1}^{n_p(t)} S_{\phi j}} (1 - \eta_{T\phi})(X(t) - T\phi) \quad (5)$$

where ϕj is the location of promoter j , $n_{pT\phi}$ is the number of T7 RNA polymerase promoters before the terminator $T\phi$, $\eta_{T\phi}$ is the efficiency of termination, and $T\phi$ is the location of the terminator. The two indices, j and k , refer to the gp1 promoters. This equation elaborates on Equation (2) by utilizing $S_{\phi j}$ to calculate a weighted average transcript length and a second term to account for read-through at $T\phi$. This second term is nonzero only after $T\phi$ has entered the host, that is, for $X(t) - T\phi$ greater than zero. Figure 3(b) provides a depiction of the terms from Equation (5). For the promoters upstream of $T\phi$, $X(t)$ in the first term will equal $T\phi$ after $T\phi$ has entered the cell.

Table II. T7 RNA polymerase promoter data^a used in the simulation.

Promoter	Relative strength ^b	Initiation efficiency	$S_{\phi j}$ ^c
$\phi 1.1A$	0.15 ^d	0.296 ^e	0.044
$\phi 1.1B$	0.34	0.361	0.123
$\phi 1.3$	0.045	0.163	0.007
$\phi 1.5$	0.15 ^d	0.296 ^e	0.044
$\phi 1.6$	0.15 ^d	0.296 ^e	0.044
$\phi 2.5$	0.15 ^d	0.296 ^e	0.044
$\phi 3.8$	0.07	0.364	0.025
$\phi 4c$	0.15 ^d	0.296 ^e	0.044
$\phi 4.3$	0.15 ^d	0.296 ^e	0.044
$\phi 4.7$	0.15 ^d	0.296 ^e	0.044
$\phi 6.5$	0.61	0.748	0.456
$\phi 9$	0.80 ^f	0.721 ^g	0.577
$\phi 10$	1.00	0.681	0.681
$\phi 13$	0.79	0.734	0.580
$\phi 17$	0.80 ^f	0.721 ^g	0.577

^aRelative strength and initiation efficiency data taken from Ikeda, 1992.

^bAll promoter strengths are scaled relative to $\phi 10$.

^c $S_{\phi j}$ is the product of the relative strength and the initiation efficiency.

^d0.15 is the average strength of the three class II promoters.

^e0.296 is the average initiation efficiency of the three class II promoters.

^f0.80 is the average strength of the three class III promoters.

^g0.721 is the average initiation efficiency of the three class III promoters.

Translation of T7 mRNA

Translation is simulated assuming an environment of unlimited amino acids and ribosomes. We also assume that the rate at which ribosomes incorporate amino acids is constant over all T7 mRNA. The effect of RNase III processing of T7 mRNA on specific protein synthesis rates (Dunn and Studier, 1973) is not included in the simulation. From these assumptions, a general protein rate expression is developed that accounts for protein synthesis, decay, and phage particle assembly:

$$\frac{d(\text{gpi})}{dt} = \frac{(R_i)(k_R)(\text{mRNA}_i)}{L_i} - (k_{\text{dgp}})(\text{gpi}) + T_i \quad \text{for } i = 0.3, \dots, 19.5 \quad (6)$$

where gpi is the concentration of the protein i , R_i is the number of ribosomes per transcript, k_R is the rate of elongation, L_i is the length of gpi , and k_{dgp} is the protein decay rate. The total number of ribosomes active on a specific T7 mRNA is calculated using data for the spacing of ribosomes, S_r , on mRNA as a function of the *E. coli* growth rate prior to infection (Dennis and Bremmer, 1973, 1974). Lacking specific data, k_{dgp} is assumed to be constant for all T7 proteins. The term T_i , defined later, accounts for proteins that either play a direct role in procapsid assembly or are physically incorporated into the phage particle. All other gene products have T_i equal to zero.

Inactivation of RNA Polymerases

Both EcRNAP and gp1 are influenced by protein-protein interactions that reduce their transcription activities. EcRNAP is affected by the protein kinase (gp0.7) and the EcRNAP inactivation protein (gp2) while gp1 is inhibited by gp3.5. The effects of gp2 and gp3.5 are simulated using equilibrium binding constants (K_{eq}) we derive from experimental data. These calculations assume that the polymerase-inhibitor complex has no residual transcription activity and that the inhibitor can complex both free and DNA-associated polymerase equally well. Gp2-mediated inactivation is simulated using a $K_{\text{eq}1}$ equal to $5.0 \times 10^7 M^{-1}$, calculated from published data (Hesselbach and Nakada, 1977a). Inactivation of *E. coli* RNA polymerase via gp0.7 is due to an unknown mechanism but is independent of the gp0.7 kinase activity (Robertson and Nicholson, 1992; Rothman-Denes et al., 1973). Consequently, we assume the effect of gp0.7 on EcRNAP is due to the formation of a one-to-one complex and choose an equilibrium constant $K_{\text{eq}2}$ equal to $5.5 \times 10^6 M^{-1}$, which is consistent with available data (Hesselbach and Nakada, 1977b). Allocation of EcRNAP inactivation between gp0.7 and gp2 is accomplished by assigning 30% to gp0.7 and 70% to gp2 (Hesselbach and Nakada, 1977b). The simulation also modifies the total concentration of EcRNAP with a first-order protein decay function. Inhibition of gp1 by gp3.5 is simulated using a $K_{\text{eq}3}$ equal to $1.5 \times 10^7 M^{-1}$. We derived this value from the available in vitro data (Ikeda and Bailey, 1992).

Using these equilibrium relationships, the concentrations of free and complexed EcRNAP and gp1 are calculated at each point in time.

DNA Degradation and Synthesis

The release of soluble nucleotides from the digestion of *E. coli* DNA by the T7 endonuclease (gp3) and exonuclease (gp6) is simulated using a constant release rate of 32,357 *E. coli* DNA nucleotides per second from 7.5 to 15 min after the start of infection (Sadowski and Kerr, 1970). To calculate this number, we use the *E. coli* culture growth rate in T-broth at 30°C (one doubling per hour) to estimate the number of bacterial genomes per cell (1.84 genomes per cell, Bremer and Dennis, 1996) at 4.655×10^6 bp per genome (Berlyn et al., 1996). During a T7 infection approximately 85% of the *E. coli* DNA is degraded by gp3 and gp6 (Sadowski and Kerr, 1970). Lacking specific data for the rate of digestion by gp3 and gp6, we employ a constant digestion rate for the entire 450 s (7.5–15 min). Thus, $(1.84 \text{ genomes/cell}) \times (4.655 \times 10^6 \text{ bp/genome}) \times (0.85) \times (1/450 \text{ s}) \times (2 \text{ nucleotides/bp})$ yields 32,357 nucleotides per second. The simulation currently ignores other potential sources of T7 DNA precursors, such as from ribonucleotide reduction, which are probably insignificant. For example, minicells lacking chromosomal and episomal DNA have been shown to support T7 infection but produce only four progeny per infected cell (Ponta et al., 1977).

DNA synthesis is simulated by taking elongation as the rate-limiting step. The rate expression for T7 DNA depends on the concentration of T7 DNA polymerase (gp5) and the rate of progeny formation:

$$\frac{d(\text{DNA})}{dt} = \frac{(d\text{NTP})(k_{\text{PD}})(\text{gp5})}{(d\text{NTP} + K_m)(L_{\text{DNA}})} - (k_{\text{pk}})(P_{\text{R}}) \quad (7)$$

where dNTP is the concentration of free deoxynucleotides, k_{PD} is the rate of DNA elongation, gp5 is the T7 DNA polymerase concentration, K_m is the half-maximum velocity constant for gp5, L_{DNA} is the length of T7 DNA, k_{pk} is the mature DNA packaging rate, and P_{R} is the limiting species for progeny formation (procapsids or DNA). Although a primase/helicase (gp4) is required for replication (Studier, 1972), it is produced slightly earlier than gp5 in the growth cycle, and we assume it has a negligible effect on the rate of replication during a T7-WT infection. Because Equation (7) assumes each gp5 molecule is active, the simulated T7 DNA replication rate is based on multiple replication forks. As with gp1, the initial concentration of gp5 is zero and then increases as gene 5 is expressed.

Particle Assembly and DNA Packaging

Procapsid assembly is simulated with a 4.78-order nucleation-limited reaction developed from data for phage P22 (Prevelige et al., 1993). T7 and P22, both *Podoviridae*, have dissimilar genomes and growth cycles (Hausmann, 1988),

but their icosahedral capsids are both approximately 60 nm in diameter and are attached to short noncontractile tails (Ackermann and Berthiaume, 1995). The kinetic data for P22 procapsid assembly are the most comprehensive for any phage and allow the development of a procapsid (PC) rate expression:

$$\frac{d(\text{PC})}{dt} = \frac{(k_{\text{as}})(\text{gp10A})^{4.78}}{N_c} - (k_{\text{pk}})(P_{\text{R}}) \quad (8)$$

where k_{as} is the procapsid assembly rate we derived from experimental data (Prevelige et al., 1993) and N_c is the number of gp10A (major capsid protein) per procapsid. The first term, representing the formation of procapsids, is only included for gp10A concentrations above the nucleation requirement, C_N . The second term is the consumption of procapsids as progeny are formed. This last step requires complete procapsids, T7 DNA, and enough of each structural protein to complete the phage. As procapsids and progeny phage particles are assembled, the additional term, T_i , from Equation (6) accounts for the utilization of T7 proteins:

$$T_i = -(N_s) \left(\frac{(k_{\text{as}})(\text{gp10A})^{4.78}}{N_c} \right) \quad \text{for } i = 9 \quad (9a)$$

$$T_i = -(k_{\text{as}})(\text{gp10A})^{4.78} \quad \text{for } i = 10A \text{ and } [\text{gp10A}] > C_N \quad (9b)$$

$$T_i = -(N_i)(N_G)(k_{\text{pk}})(P_{\text{R}}) \quad \text{for } i = 11, \dots, 17 \quad (9c)$$

where N_s is the number of scaffolding proteins (gp9) per procapsid, C_N is the concentration of gp10A required for procapsid nucleation, N_i is the number of gp*i* per progeny phage, and N_G is the number of progeny phage per genome or procapsid. Equation (9a) accounts for the utilization of scaffolding protein during procapsid assembly. Unlike P22, which is known to recycle its scaffolding protein (Prevelige et al., 1993), T7 does not recycle gp9 (Roeder and Sadowski, 1977), despite the fact that gp9 does not remain in the final phage particle (Steven and Trus, 1986). Equations (9b)–(9c) represent incorporation of phage particle proteins into progeny. The simulation assumes that packaging of DNA into the procapsid is the rate-limiting step for T7 progeny formation:

$$\frac{d(\text{T7})}{dt} = (N_G)(k_{\text{pk}})(P_{\text{R}}) \quad (10)$$

where T7 is the number of progeny phage per cell.

In summary, the simulation accounts for the transcription and translation of 52 T7 genes. Of these 52, 15 of the best characterized gene products (0.7, 1, 2, 3.5, 5, 8, 9, 10A, 11, 12, 13, 14, 15, 16, and 17) contribute further to the simulation based on their roles in catalytic, complexation, or virion assembly processes.

RESULTS

Transcription Capacity Shifts from Host to Virus

The simulation is tested against experimental results from the early, middle, and late stages of the T7 growth cycle. Early stage data for the transcription capacity of the host and phage RNA polymerases are presented (Fig. 4A). Each data series has been scaled to its maximum value. During the first 5 min of phage DNA entry EcRNAP actively transcribes the early phage genes, including gp1. However, between 5 and 10 min, its activity drops to zero and the activity of gp1, initially zero, rises to its maximum value. The simulation performs well in capturing the shift in transcription activity from the host to the phage.

The shape of the simulated gp1 curve can be understood by considering the simulated intracellular concentrations of gene 0.7, 1, 2, and 3.5 mRNA and their respective protein species, as well as those of EcRNAP and the [gp1-gp3.5]

complex. The shoulder in the simulated gp1 transcription capacity at 5 min is due to the strong initial expression of gp3.5 which binds and inhibits gp1. This occurs as the gene 3.5 DNA enters the cell and gp1 is focused on its expression. The simulated synthesis rate of gene 3.5 mRNA (Fig. 4B) illustrates this effect. With the insertion of more T7 DNA, the active gp1 is redistributed to the stronger gp1 promoters downstream of gene 3.5. This redistribution of gp1 causes a decrease in the gene 3.5 mRNA transcription rate that correlates with the insertion of downstream gp1 promoters into the cell. During this period expression of gene 3.5 continues, but at a reduced rate relative to gene 1. The change in the rate of expression shifts the equilibrium concentrations of gp1 and gp3.5 and allows the active gp1 concentration to increase (Fig. 4C). The situation reverses after 11 min when gene 1 transcription is stopped via inhibition of EcRNAP by gp0.7 and gp2, but gene 3.5 transcription continues, albeit at a reduced rate. This causes the synthesis rate of gp3.5 to exceed that of gp1 and, due to

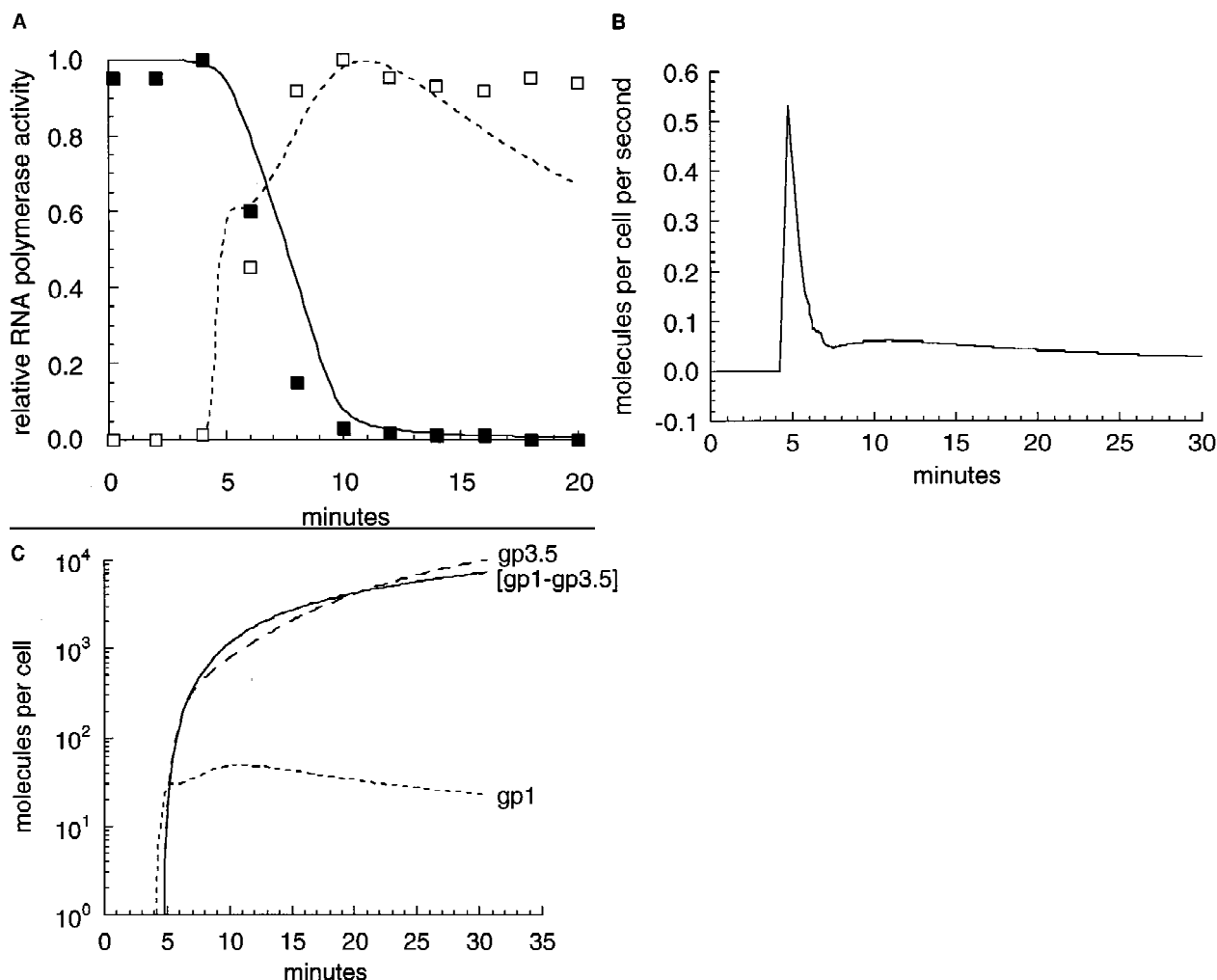


Figure 4. (A) Shift of transcription capacity, from host to phage. Experimental (Hesselbach and Nakada, 1977a) and simulated mRNA synthesis capacity. Filled squares (experimental) and solid line (simulated) are EcRNAP. Empty squares (experimental) and dashed line (simulated) are gp1. Each series is scaled relative to its maximum values. (B) Rate of gene 3.5 mRNA synthesis predicted by the T7-WT simulation. (C) Simulated intracellular concentrations of free gp1 (small dashes), free gp3.5 (large dashes), and the [gp1-gp3.5] complex (solid line).

formation of the [gp1–gp3.5] complex, reduces the concentration of active gp1 after 11 min (Fig. 4A).

Effect of Promoter Location and Strength on Simulated Gene Expression

The intracellular concentrations of 52 T7 gene products are predicted by the simulation. Factors influencing the timing and level of gene expression include DNA insertion rates, promoter strengths, and protein–protein interactions. Figure 5A illustrates how genes positioned downstream from the entering end of the genome appear at ever later times in the growth cycle (i.e., gene *I* is expressed after gene *0.3* and so on). The total expression of gene *0.3* mRNA is predicted to exceed that of gene *I* because gene *0.3* expression starts earlier in the growth cycle, when more EcRNAP is active. The stability of T7 mRNA transcripts is illustrated by the constant concentrations of gene *0.3* and gene *I* mRNA at the end of the growth cycle. The simulated concentration of class III mRNA continues to increase because a low level of active gp1 remains through the end of the growth cycle. Expression of gene *10A* mRNA exceeds all others because the polycistronic transcripts originating from upstream gp1 promoters all contain gene *10* mRNA and because the available *in vitro* data indicate that $\phi 10$, the promoter immediately upstream of gene *10A*, is the strongest on the genome (Ikeda, 1992).

The simulation is compared with experimental data for the protein synthesis initiation times of 22 gene products (Fig. 5B). Temporal resolution of the experimental data,

indicated by the horizontal bars, is limited by the 1- or 2-min intervals used in the pulse labeling experiments (Garcia and Molineux, 1995; Studier and Dunn, 1983). The simulation employs a user-defined resolution (usually 0.1–1 s) to record the time of protein synthesis initiation once the level of *gpi* exceeds one protein per cell. The solid line at 45° passing through the origin ($y = x$) indicates where the simulation would exactly match the experimental data. The plot indicates that the simulation lags behind the experimental data for the synthesis of class I proteins, with the exception of gp1.3. Then, excluding gp5, the simulation predicts synthesis of the class II and class III proteins begins earlier than the experimental data indicate. These discrepancies are discussed later.

Formation of Intracellular Phage

We performed one-step growth experiments to examine the formation of intracellular progeny phage (Fig. 6). Data were collected for two cases: T7-WT growth on BL21 and T7-26 growth on BL21(DE2). Growth of T7-26 on BL21(DE2) was simulated by setting the initial concentrations of gene *I* mRNA and gp1 equal to the final concentrations obtained from a simulation of T7-WT growth on BL21 and by deleting the region of T7 DNA coding for gene *0.7* and gene *I*. For both strains, the data show an initial lag period as T7 DNA is inserted and replicated. This is followed by the exponential increase of intracellular progeny until cellular resources become limiting and the growth curves begin to

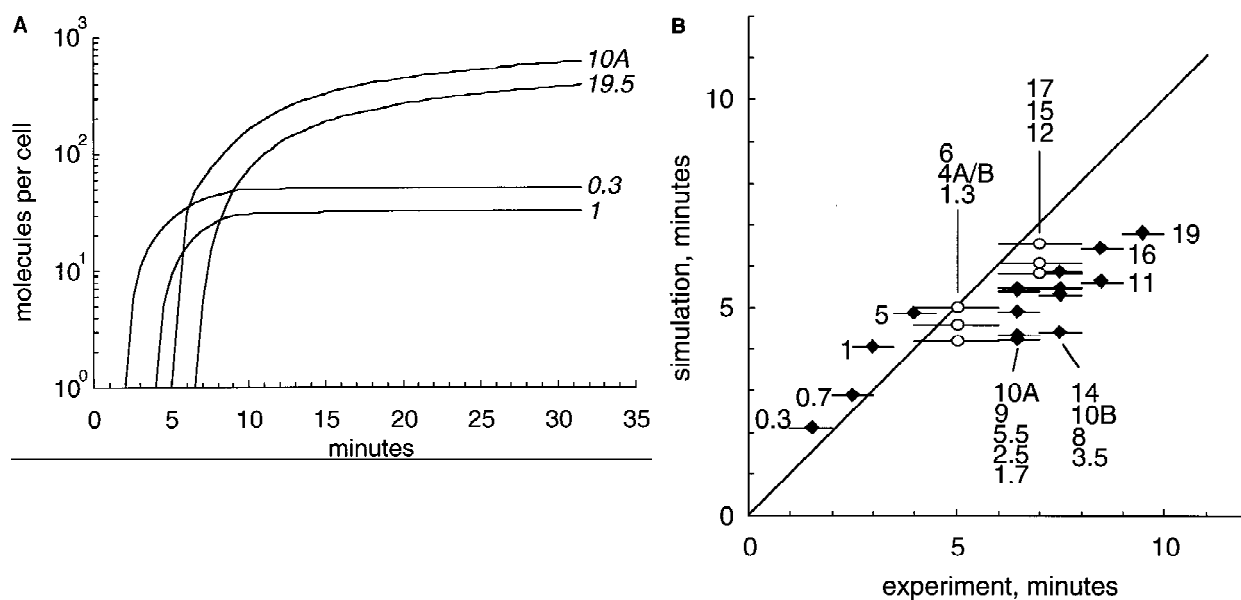


Figure 5. (A) Simulated intracellular concentrations of selected class I and class III T7 mRNA. (B) Experimental and simulated initiation of protein synthesis for a T7-WT infection. Open circles are derived from a 2-min interval pulse labeling experiment with T7-WT infecting an *E. coli* C culture growing in minimal media (Studier and Dunn, 1983). Filled diamonds are taken from a 1-min interval pulse labeling experiment with sRK836 (T7-WT carrying four GATC sites inserted at nucleotide 836) infecting an UV-irradiated culture of IJ1133(pTP166) (IJ1133 is *E. coli* K-12 strain RV $\Delta lacX74 thi \Delta(mcrC-mrr)102::Tn10$; pTP166 overproduces Dam methylase; Garcia and Molineux, 1995). Experimental times are taken from the first discernible band on polyacrylamide gel. Simulated times were recorded when the predicted *gpi* level exceeded 1.0. The solid line indicates where the simulation and experiment would exactly match.

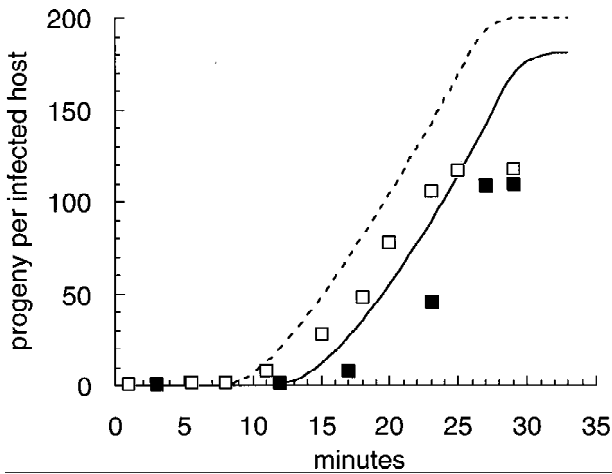


Figure 6. Intracellular one-step growth results for two T7 strains. Filled squares (experimental) and solid line (simulated) are T7-WT infecting BL21. Empty squares (experimental) and dashed line (simulated) are T7-26 infecting BL21(DE2).

plateau. Both of the experimental growth curves level off at a plateau approximately 40% below the simulated plateau. This discrepancy is most likely due to the incomplete packaging of newly replicated DNA during an actual infection. Examination of extracts after host cell lysis usually reveal that only 25–50% of the replicated DNA is packaged (personal communication, I. J. Molineux) whereas the simulation assumes all replicated T7 DNA is packaged to yield viable phage progeny.

The differences between the two growth curves may be attributed to several factors. First, the availability of gp1 at the start of the infection on BL21(DE2) may enable earlier class II and class III gene expression than in BL21. This would occur from either an earlier recognition of the ϕOL or $\phi I.A$ promoters by gp1, which would increase the translocation rate, or a higher transcription level of class II and III genes due to a higher gp1 concentration. Second, the reduced length of the T7-26 genome would shorten translocation and packaging times and, on a stoichiometric basis, would allow for more replicated genomes relative to a T7-WT infection (fewer nucleotides per progeny genome). Finally, since T7-26 does not inhibit EcRNAP via gp0.7, stronger expression of gene *I* may increase the expression rate of the class II and III genes. In agreement with this last hypothesis, previous work has shown that laboratory cultures of T7 $\Delta 0.7$ strains grow faster than T7-WT (Kong and Yin, 1995; Studier et al., 1979).

Exploring Potential Antiviral Strategies

The simulation provides a useful tool for predicting how drugs that target specific components of the virus may influence its growth. Here, one class of drugs, antisense RNA (Murray, 1992), is explored because of its potential application to medically important viruses such as HIV-1 (Bordier et al., 1995; Chatterjee et al., 1992). The inclusion of

antisense RNA in the simulation is accomplished using four simplifying approximations: (1) All antisense immediately and irreversibly binds its target mRNA. The effects of binding kinetics and incomplete antisense binding to the target are ignored. (2) The total concentration of antisense is defined at the start of infection and does not increase or decay over the course of the growth cycle. (3) Formation of duplex RNA that prevents translation of one gene is assumed to have no effect on the translation of downstream genes. (4) Binding of the antisense to T7 mRNA is not blocked by ribosomes. Each of these approximations may be readily modified to account for more detailed antisense–mRNA interactions.

Figure 7 shows T7 growth in the presence and absence of antisense that targets gene *10A* mRNA. The concentration of antisense (43 molecules per cell) is 10% of the total gene *10A* mRNA concentration synthesized during a normal T7-WT growth cycle. This antisense dose negates only the initial expression of gene *10A* causing the lag time for the synthesis of gp10A to increase from 6 to 7.5 min. In turn, this causes a lag in procapsid formation and finally a lag in the production of progeny phage. The increase in procapsid concentration seen at the end of both growth cycles is due to the complete packaging of replicated T7 DNA, which eliminates the depletion of procapsids caused by progeny formation.

To search for effective antisense strategies, the simulation was modified to target different T7 mRNA over a range of antisense concentrations. By solving the simulation for each combination of antisense target and dose, a range of growth cycle responses were found. Figure 8 gives results for antisense strategies representative of the 15 T7 genes that have a kinetic or stoichiometric role in the simulation. As a basis for comparison, the time required to produce 99%

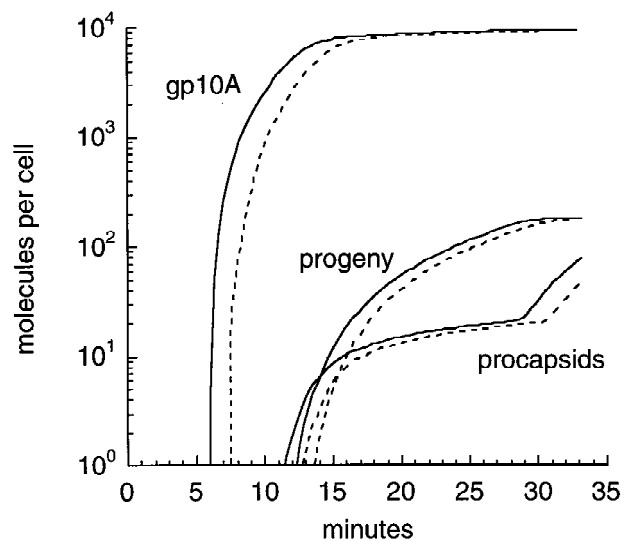


Figure 7. Comparison of the simulated intracellular gp10A, procapsid, and progeny concentrations for a T7-WT growth cycle (solid lines) and a T7-WT growth cycle modified with 43 gene *10A* antisense RNA (dashed lines).

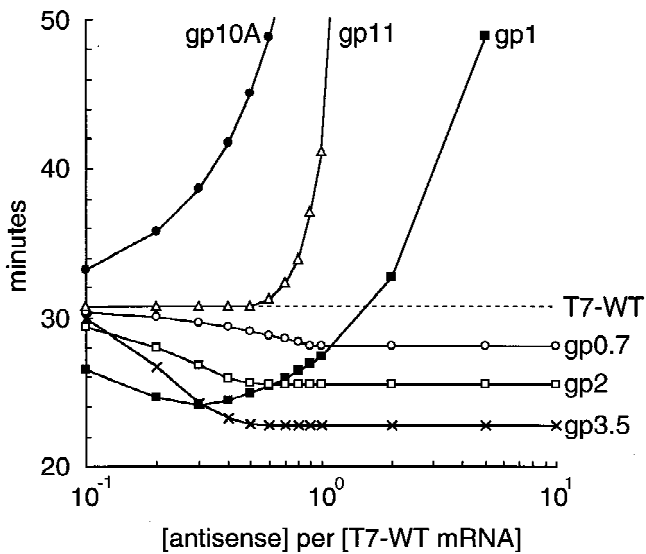


Figure 8. Simulated effect of selected antisense on the T7 growth cycle. Antisense concentrations are given relative to mRNA concentrations at the end of the T7-WT growth cycle (Table III). The Y axis indicates the time required to produce 99% of T7-WT progeny as defined by the intracellular one-step growth experiments (~115 progeny). The dashed line shows the time for the T7-WT growth cycle (30.75 min).

of the T7-WT burst (taken from the intracellular one-step growth experiments, ~115 progeny) was calculated for each antisense molecule over a range of concentrations and plotted on the ordinate. Antisense strategies that inhibit T7 growth produce curves above the dashed line, while those which enhance growth are shown below the line. Antisense against gene *10A* mRNA is predicted to have the greatest relative inhibition of T7 followed by antisense against gene *11* mRNA. The gene *11* mRNA curve is representative of antisense directed against other phage particle mRNAs (gene 8, 12, 13, 14, 15, 16, and 17 mRNA; data not shown). The curve for gene *1* mRNA predicts low antisense concentrations would accelerate phage growth relative to wild-type while higher antisense concentrations would inhibit phage growth. Since gp0.7, gp2, and gp3.5 exert negative feedbacks on the host and phage RNA polymerases, antisense directed against their respective mRNAs are predicted to enhance T7 growth. It should be noted that the gene 3.5 antisense mRNA curve does not account for the effect gp3.5 may have on DNA replication (Studier, 1972) or its role in

Table III. Intracellular mRNA concentration.

Gene	mRNA (molecules/cell) ^a
<i>0.7</i>	40
<i>1</i>	30
<i>2</i>	87
<i>3.5</i>	97
<i>10A</i>	434
<i>11</i>	64

^aSimulated concentration 30.75 min postinfection in a T7-WT growth cycle.

lysis. The enhancement of the growth rate due to the inhibition of gene *0.7* mRNA is in agreement with experiments for T7 $\Delta 0.7$ strains (Kong and Yin, 1995).

DISCUSSION

The simulation captures many important characteristics of the phage growth cycle, including the redirection of resources from host to phage, the controlled expression of phage genes, and the sharp rise of intracellular phage progeny. In addition, we have demonstrated the potential power of such a simulation to provide insights for the design of antiviral strategies. The simulation remains a work in progress. As details of the T7 growth cycle are further revealed, the simulation will be modified and improved. We hope, however, that this current simulation will facilitate future study of T7 by providing a tool for proposing and quantitatively testing hypothetical mechanisms as illustrated below.

Sharp Down Regulation of T7 RNA Polymerase Activity

A discrepancy exists after 12 min between the simulated *in vivo* data and experimental measured *in vitro* data for transcription capacity (Fig. 4A). This occurs because the simulation continues to express gene 3.5 beyond 12 min. Since EcRNAP is inactive, gene *1* mRNA is no longer being produced. Consequently the gp3.5 concentration increases relative to gp1 and the simulated concentration of active gp1 decreases due to complexation with gp3.5. Without this decrease the simulation would match the experimental *in vitro* data. However, it is unlikely this mechanism accounts for the discrepancy because other experimental data show translation of gene *1* mRNA stops 8 min into the growth cycle (Garcia and Molineux, 1995; Studier and Dunn, 1983). Thus, regardless of the gene *1* mRNA concentration, the concentration of gp3.5 will increase relative to gp1.

Data for the *in vivo* T7 transcription capacity indicate that all transcription in a T7-WT infection is effectively completed by 12 min (McAllister and Wu, 1978; Zhang and Studier, 1995). To match this *in vivo* data, a more detailed mechanism is required. One hypothesis is that the 12-min cutoff of transcription seen *in vivo* results from the [gp1-gp3.5] complex binding T7 DNA at the gp1 promoters and preventing transcription. In other words, as [gp1-gp3.5] complexes form, they block transcription by binding the gp1 promoters and preventing free gp1 from initiating new transcripts. This mechanism would allow lower concentrations of gp3.5 to inhibit gp1-mediated transcription. Such a hypothesis has been simulated using the mechanisms and kinetic rates given in Figure 9. Figure 10 indicates that the revised active gp1 concentration predicted by this simulation matches the experimental data (Zhang and Studier, 1995) quite well. It should be noted that the first 5 min of experimental data, which represents transcription by the EcRNAP, should not be expected to match the simulated

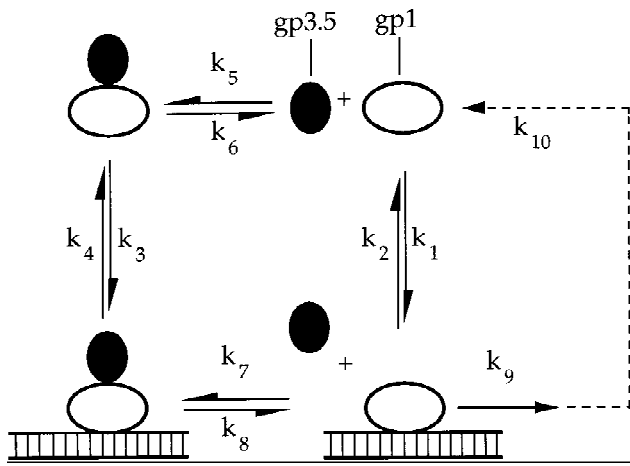


Figure 9. Hypothesized mechanism for the interaction of gp1, gp3.5, and gp1 promoters. [gp1-gp3.5] binding is assumed to be independent of gp1 binding to a promoter and vice versa. Therefore, we choose $k_1 = k_3$ ($1 \times 10^9 M^{-1} s^{-1}$), $k_2 = k_4$ ($1.5 s^{-1}$), $k_5 = k_7$ ($1.5 \times 10^4 M^{-1} s^{-1}$), and $k_6 = k_8$ ($1 \times 10^3 s^{-1}$). The term k_9 ($0.5 s^{-1}$) represents the rate of isomerization from bound to elongating gp1. The dashed line and k_{10} ($0.167 s^{-1}$) indicate the transit time and recycle rate of gp1, respectively.

gp1 activity. The details of this mechanism have yet to be experimentally verified.

In vivo T7 RNA Polymerase Promoter Differences

T7 class III promoters are stronger than the class II promoters in vitro (Ikeda, 1992). We expect this difference in promoter strengths will be significant in vivo if the T7 promoters compete for active gp1. However, if the concentration of active gp1 is high, then the promoter sites should be gp1-saturated and differences in transcription rates would be primarily due to differences in promoter clearance rates. To estimate if active gp1 enzyme is in excess, we divide the

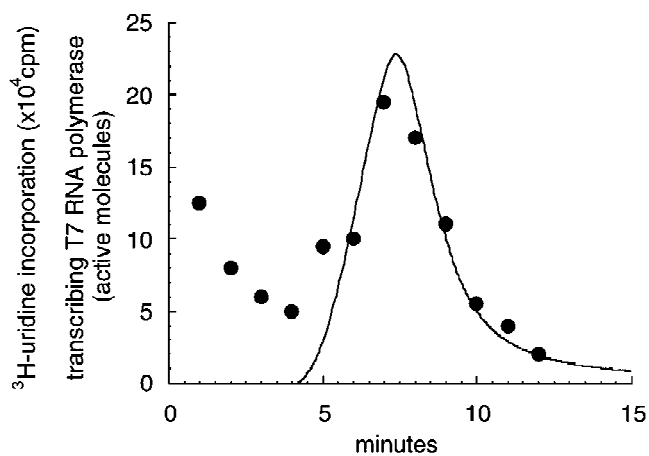


Figure 10. T7 RNA polymerase activity. In vivo ³H-uridine incorporation (filled circles; Zhang and Studier, 1995) and simulated gp1 activity (solid line). This prediction uses data for the concentrations of gp1 and gp3.5 from the T7-WT simulation as input. The experimental data include EcRNAP activity from 0 to 5 min.

length of inserted class II and class III DNA by the EcRNAP spacing requirement. This provides a first-order approximation for the “saturating” concentration of active gp1 (approximately 112 molecules per cell when all T7 DNA is inserted). The maximum active gp1 concentration calculated by the simulation approaches 50 molecules per cell (Fig. 4C), well below the saturating concentration. This supports the hypothesis that the increase in strength from class II to class III promoters observed in vitro will by competition shift transcription from class II to class III genes in vivo.

T7 Protein Synthesis Initiation and DNA Translocation

Previous simulations (Buchholtz and Schneider, 1987) demonstrated that the time required for a given gene *i* to enter the host creates a lag time in the growth cycle for its expression. Here, the translocation mechanism has been updated with recent DNA insertion rate data (Garcia and Molineux, 1995) and applied to all T7 genes. The resulting simulated protein synthesis initiation times are compared with experimental data for 22 T7 proteins. The delay in the simulated protein synthesis initiation times for the class I genes may be caused by a rate of DNA ejection during the first stage of translocation that is too slow. More recent data indicate that the 5-bps rate for the initial DNA region is a minimum value and that the actual translocation rate may be 10-fold or more higher (I. J. Molineux, personal communication). Increasing this rate would shorten the simulated initiation times of class I protein synthesis, possibly improving their match with experimental data in Figure 5B.

The discrepancy between the simulated and experimental synthesis initiation times for the class II and class III proteins may be explained by several hypothetical mechanisms. First, there may be a lag in the recognition of $\phi I.1A$ by the first molecules of gp1. Incorporating this mechanism would cause a delay in the translocation rate increase (from 40 to 200 bps) and produce a step increase in the simulated initiation times of most class II and class III genes. The early class II genes should not be affected because translocation would still occur at the EcRNAP-mediated rate of 40 bps. Second, if gp1 were unable to effectively mediate translocation at its elongation rate but could pull T7 DNA into the host at a rate below 200 bps, the simulated initiation times would lengthen. Further, the effect of this mechanism would increase over the length of the class II and class III DNA. The effective rate of gp1-mediated translocation that would produce agreement between simulated and experimental initiation times is approximately 100 bps or 50% of the gp1 elongation rate currently used in the simulation. Finally, it is possible that gp16 acts as a molecular brake during the early stages of DNA translocation (I. J. Molineux, personal communication). Any delay in translocation resulting from this mechanism would increase the current discrepancy between simulated and experimental data for the class I proteins (Fig. 5B) but improve the fit with the class II and class III pro-

teins in a manner similar to the potential gp1- ϕ 1A mechanism.

Down Regulation of T7 mRNA Translation

The simulation cannot yet account for the sharp inhibition of translation seen for some class I and class II mRNA (e.g., gene 1 and 2.5 mRNA; Studier and Dunn, 1983). Since T7 mRNA are thought to be stable over the course of the growth cycle (Summers, 1970) and no agents have been identified which inhibit translation from specific T7 transcripts, the mechanism for this process remains unknown. What is clear, however, is that the continued simulated translation of T7 mRNA until the end of the growth cycle does not agree with available experimental data.

Exploration of Antiviral Strategies

In addition to unifying the available mechanistic and kinetic data for the T7 growth cycle, the simulation provides a framework for quantitatively evaluating how well-defined viral mutations or drug targeting of specific viral components influence the growth process. By simulating the metabolism of the infection, we provide a way to predict potential complications, as well as opportunities for gaining insights into the global effects of a particular strategy. This approach should help drug designers anticipate system-level responses and may explain the unanticipated behavior of some antisense strategies observed in vivo (Gura, 1995). For example, we have shown that strategies inhibiting an essential component of T7 (gene 1 mRNA) may accelerate T7 growth. In addition, the simulation predicts how target selection leads to accelerated and inhibited phage growth. As mechanisms and data become available for the activity and localization of antisense in vivo, we anticipate that extensions of this approach will provide insights for the design of antiviral strategies against eukaryotic viruses.

CONCLUSIONS

Despite the predominately qualitative and reductionist focus of molecular biology (Maddox, 1992), our results suggest that a quantitative and synthetic perspective can provide a valuable tool for exploring viral growth at the molecular level. Using a chemical-kinetic framework, we have consolidated data on the molecular physiology of phage T7 and used the resulting computer simulation to explore the rich dynamics of phage growth. As the fundamental database expands, the simulation will be adapted, enabling a more detailed and coherent picture of T7 dynamics to emerge. Even in its preliminary form, the simulation has suggested fertile areas for future investigations in the control of translocation, transcription, translation, and drug design. Our approach provides a foundation for creating detailed genetically structured simulations of other prokaryotic as well as eukaryotic viruses.

We thank I. J. Molineux for his comments, suggestions, and communication of unpublished results. We also thank F. W. Studier, A. Rosenberg, and X. Zhang for their helpful comments and suggestions.

NOMENCLATURE

A_j	EcRNAP promoter j (location on T7 DNA)
C_N	gp10A concentration required for nucleation (molecules/cell)
DNA	T7 DNA concentration (molecules/cell)
dNTP	dinucleotide triphosphate concentration (molecules/cell)
EcRNAPE	<i>coli</i> RNA polymerase
gpi	i th T7 gene product (molecules/cell)
i	T7 gene index (Studier and Dunn, 1983)
j, k	gp1 promoter indices
k_{1-10}	kinetic parameters defining gp1, gp3.5, and gp1 promoter kinetics
k_{as}	procapsid assembly rate [1/(molecules/cell) ^{3.78} /min]
k_{dgp}	gene product decay rate (s ⁻¹)
k_{dm}	mRNA decay rate (s ⁻¹)
K_{cq1-3}	protein-protein equilibrium constant (M^{-1})
k_{PD}	DNA polymerase elongation rate (bp/s/polymerase)
k_{Ph}	EcRNAP transcription rate (nucleotides/s/polymerase)
k_{pk}	DNA packaging rate (s ⁻¹)
k_{PT7}	gp1 transcription rate (nucleotides/s/polymerase)
k_R	ribosome translation rate (amino acids/s/ribosome)
K_m	Michaelis constant for DNA polymerase (molecules/cell)
L_i	length of gpi (amino acids/protein)
$L_H(t)$	average T7 transcript length from EcRNAP (nucleotides/mRNA)
$L_p(t)$	weighted average T7 transcript length from gp1 (nucleotides/mRNA)
L_{DNA}	length of T7 DNA (39,937 bp/genome)
mRNA $_i$	i th T7 mRNA (molecules/cell)
n_i	number of gp1 promoters upstream of gene i
$n_H(t)$	number of inserted EcRNAP promoters at time t
$n_p(t)$	number of inserted gp1 promoters at time t
$n_{pT\phi}$	number of gp1 promoters upstream of T ϕ
N_c	gp10A per procapsid (molecules/procapsid)
N_G	number of phage per genome or procapsid (phage/genome or procapsid)
N_i	number of proteins per phage (molecules/phage particle)
N_s	gp9 per procapsid (molecules/procapsid)
P_h	EcRNAP active on T7 DNA (molecules/cell)
P_R	limiting species for progeny formation, PC or DNA (molecules/cell)
P_{T7}	gp1 active on T7 DNA (molecules/cell)
PC	procapsids (molecules/cell)
R_i	number of ribosomes active on transcript i (ribosomes/mRNA)
S_i	strength of gene i 's upstream promoters
$S_{\phi j}, S_{\phi k}$	strength of promoter j or k (binding strength \times elongation efficiency)
S_p	distance between active RNAPs (bp)
S_r	distance between active ribosomes (nucleotides)
t	time (s)
T7	progeny phage (molecules/cell)
TE	position of the early EcRNAP terminator (location on T7 DNA)
T_i	additional gene product rate term (molecules/cell/s)
T ϕ	position of gp1 terminator (location on T7 DNA)
$X(t)$	marker for T7 DNA inserted at time t (location on T7 DNA)
$\eta_{T\phi}$	efficiency of gp1 terminator T ϕ
ϕ_j, ϕ_k	T7 RNA polymerase promoter j or k (location on T7 DNA)
μ	<i>E. coli</i> growth rate (h ⁻¹)

T7 proteins referred to in text

Phage particle stoichiometry data (in parentheses) from Steven and Trus, 1986.

gp0.3	antirestriction protein
gp0.7	protein kinase
gp1	T7 RNA polymerase
gp1.3	DNA ligase
gp1.7	unknown
gp2	inhibits <i>E. coli</i> RNA polymerase
gp2.5	single-stranded DNA-binding protein
gp3	endonuclease
gp3.5	lysozyme inhibits T7 RNA polymerase
gp4A/B	primase/helicase
gp5	DNA polymerase
gp5.5	permits growth on λ lysogens
gp6	exonuclease
gp8	head-tail connector protein (12/phage)
gp9	head assembly protein (137/procapsid)
gp10A/B	major/minor head protein (415/phage)
gp11	tail protein (18/phage)
gp12	tail protein (6/phage)
gp13	core protein (33/phage)
gp14	core protein (18/phage)
gp15	core protein (12/phage)
gp16	core protein (3/phage)
gp17	tail fiber protein (18/phage)
gp19	DNA maturation

References

Ackermann, H. W., Berthiaume, L. 1995. Atlas of virus diagrams. CRC Press, New York.

Adams, M. 1959. Bacteriophages. Interscience, New York.

Berlyn, M. K., Low, K. B., Rudd, K. E. 1996. Linkage map of *E. coli* K-12, edition 9, pp. 1715–1902. In: F. C. Neidhardt, R. Curtiss, III, C. Gross, J. Ingraham, E. C. C. Lin, K. B. Low, B. Magasanik, W. S. Reznikoff, M. Riley, M. Schaechter, and H. E. Umbarger, (eds.), *E. coli* and *S. typhimurium*: Cellular and molecular biology II. American Society for Microbiology, Washington DC.

Bordier, B., Perala-Heape, M., Degols, G., Lebleu, B., Litvak, S., Sarih-Cottin, L., Helene, C. 1995. Sequence-specific inhibition of human immunodeficiency virus (HIV) reverse transcription by antisense oligonucleotides: Comparative study in cell-free assays and in HIV-infected cells. *Proc. Nat. Acad. Sci. USA* **92**: 9383–9387.

Bremer, H., Dennis, P. P. 1996. Modulation of chemical composition and other parameters of the cell by growth rate, pp. 1553–1569. In: F. C. Neidhardt, R. Curtiss, III, C. Gross, J. Ingraham, E. C. C. Lin, K. B. Low, B. Magasanik, W. S. Reznikoff, M. Riley, M. Schaechter, and H. E. Umbarger (eds.), *E. coli* and *S. typhimurium*: Cellular and molecular biology II. American Society for Microbiology, Washington DC.

Bremer, H., Yuan, D. 1968. RNA chain growth-rate in *Escherichia coli*. *J. Molec. Biol.* **38**: 163–180.

Buchholtz, F., Schneider, F. W. 1987. Computer simulation of T3/T7 phage infection using lag times. *Biophys. Chem.* **26**: 171–179.

Burden, R. L., Faires, J. D. 1993. Numerical Analysis. PWS Publishing Co., Boston.

Chatterjee, S., Johnson, P. R., Wong, K. K. 1992. Dual-target inhibition of HIV-1 in vitro by means of an adeno-associated virus antisense vector. *Science* **258**: 1485–1488.

Dalbow, D. G., Young, R. 1975. Synthesis time of B-galactosidase in *Escherichia coli*. B/r as a function of growth rate. *Biochem. J.* **150**: 13–20.

Dee, K. U., Hammer, D. A., Shuler, M. L. 1995. A model of the binding,

entry, uncoating, and RNA synthesis of semliki forest virus in baby hamster kidney (BHK-21) cells. *Biotechnol Bioeng.* **46**: 485–496.

Demerec, M., Fano, U. 1944. Bacteriophage-resistant mutants in *Escherichia coli*. *Genetics* **30**: 119–136.

Dennis, P. P., Bremer, H. 1973. Regulation of ribonucleic acid synthesis in *Escherichia coli* B/r: An analysis of a shift-up I. Ribosomal RNA chain growth rates. *J. Molec. Biol.* **75**: 145–159.

Dennis, P. P., Bremer, H. 1974. Macromolecular composition during steady-state growth of *Escherichia coli* B/r. *J. Bacteriol.* **119**: 270–281.

Donachie, W. D., Robinson, A. C. 1987. Cell division: Parameter values and the process, pp. 1578–1593. In: F. C. Neidhardt, J. L. Ingraham, K. B. Low, B. Magasanik, M. Schaechter, and H. E. Umbarger (eds.) *E. coli* and *S. typhimurium*: Cellular and molecular biology. American Society for Microbiology, Washington, DC.

Donlin, M. J., Johnson, K. A. 1994. Mutants affecting nucleotide recognition by T7 DNA polymerase. *Biochemistry* **33**: 14908–14917.

Dunn, J. J., Studier, F. W. 1973. T7 early RNAs and *Escherichia coli* ribosomal RNAs are cut from large precursor RNAs *in vivo* by ribonuclease III. *Proc. Natl. Acad. Sci. USA* **70**: 3296–3300.

Dunn, J. J., Studier, F. W. 1975. Effect of RNAase III cleavage on translation of bacteriophage T7 messenger RNAs. *J. Molec. Biol.* **99**: 487–499.

Dunn, J. J., Studier, F. W. 1983. Complete nucleotide sequence of bacteriophage T7 DNA and the locations of T7 genetic elements. *J. Molec. Biol.* **166**: 477–535. Updated bacteriophage T7 sequence (T7CG) accessed from NCBI GenBank (<http://www.ncbi.nlm.nih.gov/>).

Eigen, M., Biebricher, C. K., Gebinoga, M., Gardiner, W. C. 1991. The hypercycle. Coupling of RNA and protein biosynthesis in the infection cycle of an RNA bacteriophage. *Biochemistry* **30**: 11005–11108.

Garcia, R. L., Molineux, I. J. 1995. Rate of translocation of bacteriophage T7 DNA across the membranes of *Escherichia Coli*. *J. Bacteriol.* **177**: 4066–4076.

Gura, T. 1995. Antisense has growing pains. *Science* **270**: 575–577.

Hammond, B. 1993. Quantitative study of the control of HIV-1 gene expression. *J. Theor. Biol.* **163**: 199–221.

Hausmann, R. 1988. The T7 group, pp. 259–289. In: R. Calendar (ed.), *The Bacteriophages*, vol. 1. Plenum, New York.

Hesselbach, B. A., Nakada, D. 1977a. I protein: Bacteriophage T7-coded inhibitor of *Escherichia Coli* RNA polymerase. *J. Virol.* **24**: 746–760.

Hesselbach, B. A., Nakada, D. 1977b. “Host shutoff” function of bacteriophage. T7: Involvement of T7 gene 2 and gene 0.7 in the inactivation of *Escherichia coli* RNA polymerase. *J. Virol.* **24**: 736–745.

Hillis, D. M., Bull, J. J., White, M. E., Badgett, M. R., Molineux, I. J. 1992. Experimental phylogenetics: Generation of a known phylogeny. *Science* **255**: 589–592.

Ikeda, R. A. 1992. The efficiency of promoter clearance distinguishes T7 class II and class III promoters. *J. Biol. Chem.* **267**: 11322–11328.

Ikeda, R. A., Bailey P. A. 1992. Inhibition of T7 RNA polymerase by T7 lysozyme *in vitro*. *J. Biol. Chem.* **267**: 20153–20158.

Kong, D., Yin, J. 1995. Whole-virus vaccine development by continuous culture on a complementing host. *Bio/Technology* **13**: 583–586.

Lee, S. B., Bailey, J. E. 1984. Analysis of growth rate effects on productivity of recombinant *Escherichia coli* populations using molecular mechanism models. *Biotechnol. Bioeng.* **26**: 66–73.

Lee, Y., Yin, J. 1996. Detection of evolving viruses. *Nature Biotechnol.* **14**: 491–493.

Macdonald, L. E., Zhou, Y., McAllister, W. T. 1993. Termination and slippage by bacteriophage T7 RNA polymerase. *J. Molec. Biol.* **232**: 1030–1047.

Maddox, J. 1992. Is molecular biology yet a science? *Nature* **355**: 201.

Maslak, M., Jaworski, M. D., Martin, C. T. 1993. Tests of a model for promoter recognition by T7 RNA polymerase: Thymine methyl group contacts. *Biochemistry* **32**: 4270–4274.

McAdams, H. H., Shapiro, L. 1995. Circuit simulation of genetic networks. *Science* **269**: 650–656.

McAllister, W. T., Wu, H. L. 1978. Regulation of transcription of the late genes of bacteriophage T7. *Proc. Nat. Acad. Sci. USA* **75**: 804–808.

- Miller, J. H. 1972. Experiments in molecular genetics. Cold Spring Harbor: Cold Spring Harbor Laboratory.
- Moffatt, B. A., Studier, F. W. 1988. Entry of bacteriophage T7 DNA into the cell and escape from host restriction. *J. Bacteriol.* **170**: 2095–2105.
- Murray, J. A. H. 1992. Antisense RNA and DNA. Wiley-Liss, New York.
- Palsson, B. O., Keasling, J. D., Emerson, S. G. 1990. The regulatory mechanisms of human immunodeficiency virus replication predict multiple expression rates. *Proc. Nat. Acad. Sci. USA* **87**: 772–776.
- Ponta, H., Reeve, J. N., Pfennig-Yeh, M., Hirsch-Kauffmann, M., Schweiger, M., Herlich, P. 1977. Productive T7 infection of *Escherichia coli* F+ cells and anucleate minicells. *Nature* **269**: 440–442.
- Prevelige, P. E., Thomas, D., King, J. 1993. Nucleation and growth phases in the polymerization of coat and scaffolding subunits into icosahedral procapsid shells. *Biophys. J.* **64**: 824–835.
- Rabkin, S. D., Richardson, C. C. 1990. *In vivo* analysis of the initiation of bacteriophage T7 DNA replication. *Virology* **174**: 585–592.
- Robertson, E. S., Nicholson, A. W. 1992. Phosphorylation of *Escherichia coli* translation initiation factors by the bacteriophage T7 protein kinase. *Biochemistry* **31**: 4822–4827.
- Roeder, G. S., Sadowski, P. D. 1977. Bacteriophage T7 morphogenesis: Phage-related particles in cells infected with wild-type and mutant T7 phage. *Virology* **76**: 263–285.
- Rose, J. K., Mosteller, R. D., Yanofsky, C. 1970. Tryptophan messenger ribonucleic acid elongation rates and steady-state levels of tryptophan operon enzymes under various growth conditions. *J. Molec. Biol.* **51**: 541–550.
- Rothman-Denes L. B., Muthukrishnan, S., Haselkorn, R., Studier, F. W. 1973. A T7 gene function required for shut-off of host and early T7 transcription, pp. 227–239. In: C. F. Fox and W. S. Robinson (eds.), *Virus research*. Academic, New York.
- Ruggiero, C., Giacomini, M., Varnier, O. E., Gaglio, S. 1994. A qualitative process theory based model of the HIV-1 virus–cell interaction. *Comput. Meth. Progr. Biomed.* **43**: 255–259.
- Sadowski, P. D., Kerr, C. 1970. Degradation of *Escherichia coli* B deoxyribonucleic acid after infection with deoxyribonucleic acid-defective amber mutants of bacteriophage T7. *J. Virol.* **6**: 149–155.
- Shuler, M. L., Leung, S., Dick, C. C. 1979. A mathematical model for the growth of a single bacterial cell. *Ann. NY Acad. Sci.* **326**: 35–55.
- Son, M., Watson, R. H., Serwer, P. 1993. The direction and rate of bacteriophage T7 DNA packaging *in vitro*. *Virology* **196**: 282–289.
- Steven, A. C., Trus, B. L. 1986. The structure of bacteriophage T7, pp. 1–35. In: J. R. Harris and R. W. Horne (eds.), *Electron microscopy of proteins*, vol. 5: Viral structure. Academic, London.
- Studier, F. W. 1969. The genetics and physiology of bacteriophage T7. *Virology* **39**: 562–574.
- Studier, F. W. 1972. Bacteriophage T7. *Science* **176**: 367–376.
- Studier, F. W., Dunn, J. J. 1983. Organization and expression of bacteriophage T7 DNA. *CSH Quant. Biol.* **47**: 999–1007.
- Studier, F. W., Moffatt, B. A. 1986. Use of bacteriophage T7 RNA polymerase to direct selective high-level expression of cloned genes. *J. Molec. Biol.* **189**: 113–130.
- Studier, F. W., Rosenberg, A. H., Simon, M. N., Dunn, J. J. 1979. Genetic and physical mapping in the early region of bacteriophage T7 DNA. *J. Molec. Biol.* **135**: 917–937.
- Summers, W. C. 1970. The process of infection with coliphage T7 IV. Stability of RNA in bacteriophage-infected cells. *J. Molec. Biol.* **51**: 671–678.
- Wickham, T. J., Shuler, M. L., Hammer, D. A. 1995. A simple model to predict the effectiveness of molecules that block attachment of human rhinoviruses and other viruses. *Biotechnol. Prog.* **11**: 164–170.
- Yin, J. 1993. Evolution of bacteriophage T7 in a growing plaque. *J. Bacteriol.* **175**: 1272–1277.
- Young, R. 1992. Bacteriophage lysis: Mechanism and regulation. *Microbiol. Rev.* **56**: 430–481.
- Zavriev, S. K., Shemyakin, M. F. 1982. RNA polymerase-dependent mechanism for the stepwise T7 phage DNA transport from the virion into *E. coli*. *Nucl Acids Res.* **10**: 1635–1652.
- Zhang X., Studier, F. W. 1995. Isolation of transcriptionally active mutants of T7 RNA polymerase that do not support phage growth. *J. Molec. Biol.* **250**: 156–168.
- Zlotnick, A. 1994. To build a virus capsid: An equilibrium model of the self assembly of polyhedral protein complexes. *J. Molec. Biol.* **241**: 59–67.